Title: Unraveling interindividual differences and functional consequences of gut microbial metabolism of immunosuppressants

Authors: Maral Baghai Arassi[1,2]*, Nicolai Karcher[2], Eleonora Mastrorilli[2], Matthias Gross[2], Amber Brauer-Nikonow[2], Raymund Hackett[3], David Czock[4], Burkhard Tönshoff[1], Georg Zeller[2,3]*, Michael Zimmermann[2]*

Affiliations:

[1]Department of Pediatrics I, University Children's Hospital Heidelberg; Heidelberg, Germany.

[2]Structural and Computational Biology Unit, European Molecular Biology Laboratory; Heidelberg, Germany.

[3]Leiden University Center for Infectious Diseases (LUCID), Leiden University Medical Center; Leiden, Netherlands.

[4]Department of Clinical Pharmacology and Pharmacoepidemiology, Heidelberg University Hospital; Heidelberg, Germany.

*Corresponding authors. Email: Email: maral.baghai@embl.de (MBA), georg.zeller@gmail.com (GZ), michael.zimmermann@embl.de (MZ)

One Sentence Summary: This study reveals interindividual variability in gut microbial metabolism of immunosuppressive drugs mediated by specific bacterial species and enzymes.

Abstract: A major challenge in kidney transplantation (KT) is the large interpatient variability in the pharmacokinetics of immunosuppressive drugs. Here, we explored the role of the gut microbiome in interindividual variation in immunosuppressive drug metabolism. Analysis of 38 fecal communities, including 10 from KT recipients, and 45 bacterial species against 25 drugs, revealed significant interindividual and drug-specific differences in metabolism. Notably, 15 of 16 immunosuppressants tested were metabolized by at least one microbial community, and we found specific bacterial species, such as *Bacteroides uniformis*, to be potent metabolizers. We identified 18 different metabolites for 16 drugs, including two previously undescribed metabolites for sirolimus and everolimus. Our study reveals the functional impact of microbial metabolism on key immunosuppressants, including inactivation of tacrolimus, activation and potential increase in toxicity of mycophenolate mofetil (MMF), and shows that the microbial metabolite of methylprednisolone exhibits a 2.6-fold increase in epithelial permeability compared to the parent drug. Through a gain-of-function genetic screen we identified the *B. uniformis* enzyme BACUNI_RS05305 to be responsible for MMF activation. Using machine learning to model microbial community drug metabolism, abundance features of prevalent species predicted the biotransformation of some drugs well, while for others, a priori experimental information on bacterial genes and enzyme protein structures led to improved predictions. Our research highlights the potential of gut microbiome features to explain interindividual variability in immunosuppressive therapies and sets the stage for clinical trials to identify microbiome-encoded signatures predictive of drug metabolism in KT patients.

Main Text:

INTRODUCTION

42 Kidney transplantation is an important therapy for end-stage organ disease *(1, 2)*. The
43 introduction of potent immunosuppressants, such as the calcineurin inhibitor tacrolimus and the
44 proliferation inhibitor mycophenolate mofetil (MMF), has improved the clinical outcome of
45 kidney transplantation (KT) making them a cornerstone of modern transplantation medicine.
46 However, the large interpatient variability in pharmacokinetics and pharmacodynamics represent
47 a major challenge in clinical practice *(3, 4)*. Underexposure of immunosuppressants may lead to
48 acute graft rejection, whereas overexposure bears the risk of serious drug-related side effects,
49 such as infections, nephrotoxicity, neurotoxicity and metabolic disorders *(5)*. Despite decades of
50 research aiming to predict an individual's drug pharmacokinetics, known biomarkers, such as
51 cytochrome P450 polymorphisms, have limited accuracy *(6)*. Therefore, novel insights into the
52 factors that determine the pharmacokinetics and pharmacodynamics of immunosuppressants are
53 urgently needed to optimize personalized immunosuppression in SOT.

54 One factor in drug metabolism that has recently garnered attention is the human gut
55 microbiome *(7–10)*. Bacteria, the major constituent of the complex gastrointestinal ecosystem,
56 harbor a myriad of metabolic enzymes with a tremendous potential to metabolize drugs. We have
57 previously found that a substantial fraction of drugs, including some widely used
58 immunosuppressants are metabolized by human gut bacteria *(7)*. The remarkable interindividual
59 genetic variability of human gut microbiomes, far surpassing that of human genomes, suggests
60 that the microbiome may partially contribute to differences in drug exposure and response *(11)*.
61 This is particularly relevant in the context of drugs with large interpersonal variability, such as
62 immunosuppressants *(5)*. Moreover, research indicates that gut microbial modifications of
63 immunosuppressants can influence drug elimination rates, toxicity *(12)* and efficacy *(13)*.
64 Despite these insights, a comprehensive understanding of the interindividual differences,

65 functional consequences and underlying mechanisms of gut microbial metabolism of
66 immunosuppressants is still lacking.

67 To close this knowledge gap, we assayed 25 medical drugs commonly used in solid organ
68 transplantation, with a special focus on KT, including 16 immunosuppressants for their
69 metabolism by 38 distinct human-derived gut microbial communities and 45 representative gut
70 bacterial species. These experiments revealed pronounced interindividual and drug-specific
71 differences in microbiota drug metabolism. We further observed that microbial metabolism of
72 the three key immunosuppressants used in KT – tacrolimus, MMF, and methylprednisolone, can
73 cause drug inactivation, prodrug activation, increased toxicity, and altered intestinal absorption.
74 Based on these data and employing genome-wide functional screens, we identified mechanistic
75 determinants of microbial drug metabolism, including specific bacterial species and drug-
76 metabolizing bacterial enzymes. These findings provide the basis for predicting interindividual
77 differences in drug metabolism from microbiome features.

78 **RESULTS**

79 **Subhead 1: Pronounced interindividual differences in microbial metabolism of**
80 **immunosuppressants**

81 To systematically assess potential interindividual differences in gut microbial metabolism
82 of immunosuppressive drugs, we analyzed the drug-metabolizing capacity of human gut
83 microbial communities derived from 19 individual donors, including 14 healthy adults and
84 children and 5 adult kidney transplant recipients (Fig. 1A, Table S1). The stool donors were
85 selected to provide a comprehensive representation of both the general population and transplant
86 recipients in particular. Characterizing the microbial composition through metagenomic
87 sequencing, we found them to be compositionally diverse and representative compared to a large

88 collection of human gut microbiomes (n = 3189, PERMANOVA R2 0.138%, see Fig. 1B, S1C
89 and Table S2 for details). Drug incubation under anaerobic and microaerobic (5% O_2)
90 conditions, to mimic differences in oxygen availability along the gastrointestinal tract *(14)*,
91 yielded 38 tested human-derived gut microbial communities (Fig. 1B, see S1A, B and Table S3,
92 S4 for details). We assayed the metabolism of each of the microbial communities against each of
93 the 25 drugs, including 16 common immunosuppressants, as well as the cornerstone
94 immunosuppressants tacrolimus, MMF and methylprednisolone, which are known for their
95 interindividual pharmacokinetic variability. Additionally, we incorporated 9 non-
96 immunosuppressive drugs frequently used as comedication following kidney transplantation
97 (Fig. 1C, Table S5). In order to test the metabolic potential of microbial communities *ex vivo* we
98 incubated each of the 475 community-drug combinations in quadruplicate and measured drug
99 metabolism kinetics (8 timepoints) over 12 hours by liquid chromatography-coupled mass
100 spectrometry (LC–MS, Fig. 1A). Of the 16 immunosuppressants tested, 15 were significantly
101 eliminated after incubation (>25 % reduction in abundance, FDR-corrected P value ≤0.05) by at
102 least one of the tested gut microbial communities compared to no-bacteria controls. Gut
103 microbial communities differed widely in their ability to metabolize drugs with respect to both
104 the number of immunosuppressants metabolized and the extent of metabolism of individual
105 drugs (Fig. 1D, Table S6 and S7). MMF was metabolized by the highest number of gut microbial
106 communities (32/38, 84%) followed by glucocorticoids, such as prednisolone (29/38, 76%) and
107 methylprednisolone (26/38, 68%) under both anaerobic and microaerobic conditions.
108 Additionally, we observed significant microbial metabolism of tacrolimus by 21% of the tested
109 gut microbial communities (8/38). Altogether, we found substantial microbial metabolism of the
110 most clinically relevant immunosuppressants with pronounced interindividual differences.

111 **Subhead 2: Identification of immunosuppressant-metabolizing gut bacterial species**

112 Given the large interindividual differences of gut microbial metabolism of
113 immunosuppressants, we next aimed to identify specific bacterial isolates capable of performing
114 immunosuppressant biotransformation. To this end, we assessed the metabolic activity of 45
115 selected gut bacterial species (Table S8) against our panel of 25 drugs. The selected species
116 encompass the five major phyla found in the human gut and represent on average 43.9% of the
117 total microbial abundance of the 38 human-derived microbial communities tested (see Fig. S2 for
118 details). Similarly, they were highly abundant in our reference human gut microbial
119 metagenomes with a mean relative abundance of up to 10% (Fig. 2). We additionally assayed
120 those 18 of the 45 (40%) bacterial species under microaerobic conditions, that are commonly
121 found in the upper gastrointestinal tract, including the small intestine. We found that single-
122 species bacterial cultures metabolized immunosuppressants under both anaerobic and
123 microaerobic conditions (Fig. 2, Table S9, 10). Metabolized drugs included positive controls
124 expected to be metabolized by gut bacteria, such as diltiazem by *Bacteroides thetaiotaomicron*
125 *(7)* or glucocorticoids by *Clostridium scindens (7, 15)*. The overall number of metabolized drugs
126 was higher under anaerobic compared to microaerobic conditions (20 vs 8), but this may be due
127 to the higher number of species tested under anaerobic compared to microaerobic conditions (44
128 versus 18 species). MMF, azathioprine and sirolimus were most extensively metabolized under
129 both culture conditions. Overall, these results indicate strong microbial metabolism of clinically
130 relevant immunosuppressants with pronounced species-specific differences. Furthermore, these
131 results align well with our observed drug metabolism by gut microbial communities, as 16 out of
132 the 25 tested drugs were metabolized by both gut microbial communities and species. This hence

133 provides the basis to understand drug metabolism of gut microbial communities as a functional
134 trait of its members.

135 **Subhead 3: Identification of microbial drug metabolites**

136 To identify bacteria-produced drug metabolites we leveraged insights from our prior
137 high-throughput screen *(7)* and existing literature *(16, 17)*. Mining untargeted metabolomics
138 data, we identified a total of 18 different drug metabolites for 16 different drugs (Table S11 and
139 Fig. 3A). The accumulation of a given drug metabolite varied between individuals and species
140 (Table S12, 13). Intriguingly, the accumulation of drug metabolites only partially correlated with
141 the depletion of respective parent compounds, suggesting that additional drug metabolites may
142 be produced (Fig. 3A, S3). Building on the established keto-reduction pathway that deactivates
143 tacrolimus *(13)* and structural similarities with sirolimus, and everolimus, we identified 9-
144 hydroxy-everolimus (982.587 Da) and 9-hydroxy-sirolimus (938.5606 Da) as two new drug
145 metabolites (Fig. 3B-D). This finding was corroborated by the fact that the same three microbial
146 communities were consistently the most effective in generating the respective microbial
147 metabolite of tacrolimus, sirolimus and everolimus (Fig. 3E). Moreover, the detection of both
148 metabolites was confirmed in our single-species screen (Fig. S3 and Table S14, S15 for details).
149 Taken together, the identification of 18 metabolites, including two previously unknown ones,
150 coupled with the observed interpersonal variability in metabolite production, not only enhance
151 our understanding of microbial drug interactions but also opens avenues for further research into
152 the functional implications of gut bacterial drug metabolism.

153 **Subhead 4: Intestinal transport of microbiota-produced metabolites**

154 To gain insights into the influence of microbial drug metabolism on enteric absorption, a
155 key determinant of systemic drug distribution, we used an *in vitro* approach to assess transport

156 rates of drugs and drug metabolites across a gut epithelial monolayer *(18)*. We focused on
157 methylprednisolone and its bacteria-produced metabolite hydroxymethylandrostadienedione
158 (HMADD, Fig. 4A). This selection was motivated by the pivotal clinical role of
159 methylprednisolone within the first-line immunosuppressive regimen in KT and its notable
160 variability in gut microbial metabolism (Fig. 4A). To establish an epithelial monolayer, Caco-2
161 cells were seeded into transwells and methylprednisolone as well as its bacteria-produced
162 metabolite were added to the apical epithelial side after the establishment of a stable Caco-2 cell
163 monolayer (Fig. 4C). This setup enabled independent access to both sides of the monolayer with
164 each compound incubated in quadruplicate and its transport kinetics measured every 30 minutes
165 over a time period of 5 hours using LC–MS. This analysis revealed that bacteria-produced
166 HMADD exhibited different absorption characteristics compared to its parent compound (Fig.
167 4D, Table S16). To control for the potential impact of bacterial culture supernatant on the
168 epithelial barrier, we also assayed the epithelial absorption of the pure chemical standard of both
169 the parent drug and its metabolite which confirmed our observation of faster epithelial absorption
170 of HMADD compared to methylprednisolone (Fig. S4). Indeed, quantification of the effective
171 permeability (P_{eff}) *(18)* revealed that the microbial methylprednisolone metabolite has a 2.6-fold
172 higher permeability (8.11 cm/sec) compared to the parent drug (3.11 cm/sec, p=0.029, see also
173 Fig. S4 for details). Collectively, these findings suggest that microbiota-produced metabolites,
174 such as HMADD, may exhibit distinct absorption rates compared to their parent drugs across gut
175 epithelial barriers, implying the possibility of systemic absorption from the large intestine,
176 potentially impacting drug pharmacokinetics.

177 **Subhead 5: Identification of immunosuppressant-metabolizing bacterial enzymes**

178 To identify the genetic determinants of gut bacterial drug metabolism, we focused on
179 MMF due to reported gastrointestinal toxicity attributed to its active moiety, MPA *(12)*.
180 Intriguingly, we found that MMF is metabolized by 16 different microbial communities (Fig.
181 5A) and 23 individual bacterial species under anaerobic conditions including the strong MMF-
182 metabolizer *Bacteroides uniformis* (Fig. 5B). To elucidate the genetic basis of gut microbial drug
183 metabolism we employed a previously established gain-of-function approach using *B. uniformis*
184 *(7)*. In brief, we extracted and sheared genomic DNA (gDNA) into 2-8 kb fragments. gDNA
185 fragments were then cloned into an *Escherichia coli* expression vector. Transformation and
186 arraying of individual clones yielded 26,000 transformed *E. coli* clones with an average insert
187 size of 3 kb (Fig. 5C), which translates into a 15-fold genome coverage of *B. uniformis*. Through
188 consecutive pooling of clones *(7)* and mass spectrometry-based testing for MMF metabolism, we
189 identified BACUNI_RS05305 (Fig. 5D), a microbial esterase, as an MMF-metabolizing enzyme.
190 To validate these findings, we expressed the enzyme encoded by BACUNI_RS05305 in *E. coli*
191 and demonstrated its MMF-metabolizing capability (Table S17). Furthermore, we showed that
192 deleting BACUNI_RS05305 in *B. uniformis* abolished MMF activation and that
193 complementation with promoters of different strength restored MMF metabolism of the
194 BACUNI_RS05305 knock-out strain (Fig. 5E). Additionally, we investigated
195 BACUNI_RS05310, a neighboring gene which exhibits 85% sequence similarity to RS05305.
196 Deleting BACUNI_RS05310 did not affect MMF metabolism (Fig. S5), indicating that subtle
197 structural variations in enzymes, undetectable by sequence analysis alone, could influence
198 enzyme functionality. In summary, our study has successfully identified the gene
199 BACUNI_RS05305 as a key player in the activation of the immunosuppressive prodrug MMF to
200 its active form MPA, shedding light on the genetics of this gut microbial drug metabolization and

201 suggesting molecular markers that could be used to explain interindividual variability in drug
202 metabolism.

203 **Subhead 6: Using microbial signatures to explain microbial drug metabolism**

204 We next sought to understand if community composition assessed by shotgun
205 metagenomic analysis is predictive for microbiota drug metabolism. To this end, we trained
206 random forest models to predict drug degradation (as continuous AUC values) from microbial
207 species and gene abundance profiles of the *ex vivo* communities for which drug degradation was
208 measured. Model performance was evaluated in leave-two-samples-out cross validation (treating
209 anaerobic and microaerobic measurements from the same stool sample as different data points
210 that were kept together either in the training or test subset). We contrasted these data-driven
211 predictions with the ones based on selected species and genes that could be experimentally
212 linked to specific drug metabolism in this or previous studies (Table S18) *(15, 19)*. The analysis
213 revealed pronounced differences between drugs and feature sets in how well drug metabolism
214 could be predicted. Metabolization of the structurally similar drugs tacrolimus, everolimus and
215 sirolimus could generally be predicted well (Spearman correlation between predicted and
216 measured AUC between 0.64 and 0.68) using species abundance profiles. However, taking only
217 those species as features that we identified as active metabolizers resulted in much poorer
218 predictions not distinguishable from null models built with permuted labels (Spearman's rho
219 between 0.04 and 0.14, Fig. 6A, B). In contrast, when using genes with reported activity against
220 tacrolimus, we observed much better predictions (achieving similar correlations as the species
221 models) compared to purely data-driven models based on a large set of microbial gene
222 abundances as features. Of note, given the similar metabolism of tacrolimus, everolimus, and
223 sirolimus, the genes known to influence tacrolimus metabolism predicted the metabolism of

224 sirolimus and everolimus similarly well. Feature importance analysis revealed that the models
225 based on overall species abundance profiles for tacrolimus, everolimus and sirolimus all relied
226 on a relatively small and consistent set of species as important predictors (Fig. S6). Predicting
227 gut microbial metabolism of other drugs, most notably methylprednisolone and MMF, was found
228 to be much more challenging. Only MMF predictions based on a large set of microbial gene
229 abundances as features were slightly better than randomized null models (Spearman's rho
230 between -0.26 and 0.31) and neither species containing active strains, a larger set of abundant
231 species, nor genes similar to the characterized MMF-metabolizing gene described above showed
232 significant predictive capacity. To better predict MMF community metabolism, we first
233 identified putative homologs (50% sequence identity, 50% coverage) of the MMF-metabolizing
234 esterase that we experimentally identified in the genomes of our tested species. While we
235 detected similar sequences even in species only distantly related to *B. uniformis*, the presence of
236 such homologs only poorly predicted measured MMF degradation in these species (Fig. 6E, F).
237 Motivated by this result and our observation that the closely related *B. uniformis* homolog
238 BACUNI_RS05310 (with 85% sequence similarity) lacked a comparable metabolic function, we
239 performed a structural analysis of BACUNI_RS05305 and BACUNI_RS05310 using
240 AlphaFold2. We identified key differences in the substrate binding site, notably the substitution
241 of methionine with alanine at position 191 within the oxyanion hole, alongside alterations in two
242 arginine residues (Fig. 6D). These changes may affect the surface polarity and Van der Waals
243 forces near the binding site, potentially impacting substrate specificity due to the role of the
244 oxyanion hole in stabilizing the transition state during catalysis. Extending this structural
245 analysis to the identified homologs across the tested species tended to better explain inactive
246 species in which a sequence homologue had been detected, but was not sufficient to provide an

247 explanation for all species with measured activity against MMF (Fig. 6E, F; Table S19).
248 However, larger datasets (additional species and *ex vivo* communities with measured activity
249 against MMF) will be needed to validate this approach. In summary, our study elucidates the
250 complexities of predicting microbial metabolism of immunosuppressants, driven by the diverse
251 genetics of microbial species, enzyme structures, and the chemical properties of drugs. While
252 species-level information may be sufficient for some drugs, a deeper understanding of the
253 responsible bacterial genes and structural details of enzyme-substrate interactions are crucial for
254 others.

255 **DISCUSSION**

256 Microbial drug metabolism by single gut bacterial isolates has been well-documented for
257 specific immunosuppressive drugs *(13, 16, 19)*. In this study, we expanded this knowledge by
258 systematically screening a broad range of immunosuppressive drugs of clinical relevance against
259 a diverse array of human-derived gut microbial communities and bacterial isolates. Our findings
260 revealed that nearly all immunosuppressive drugs undergo microbial biotransformation with
261 marked interindividual and drug-specific variation. Intriguingly, we did not find universally
262 strong or weak metabolizing communities, but rather that the ability of a given microbial
263 community to metabolize one specific immunosuppressive drug at best weakly predicts its
264 efficiency in metabolizing others (Fig. S7). This underscores the need to investigate gut
265 microbial metabolism for each drug individually. Understanding and predicting microbial
266 metabolism of immunosuppressive drugs in clinical settings will additionally be complicated by
267 the fact that KT patients frequently receive a combination of tacrolimus, MMF, and
268 methylprednisolone as standard first-line therapy.

269 Building on prior research that highlighted the influence of microbial metabolism on the
270 efficacy and toxicity of immunosuppressive drugs *(20, 21)*, our study further elucidates how gut
271 microbiota can modify drug responses both locally and systemically. We demonstrated that
272 bacteria can activate the prodrug MMF into its active form, mirroring the host's prodrug
273 activation. However, this bacterial activation may contribute to the gastrointestinal toxicity of
274 MMF, as the local presence of the active metabolite MPA in the gut is linked to gastrointestinal
275 adverse effects *(21)*. On the other hand, the conversion of methylprednisolone into a metabolite
276 with enhanced epithelial transport properties exemplifies the potential systemic impact of
277 microbial drug metabolism. This is consistent with other studies demonstrating the systemic
278 presence of microbial metabolites, such as the inactivated tacrolimus metabolite described above,
279 in the bloodstream *(22)*.

280 Our study of MMF, which pinpointed specific bacterial species and enzymes that
281 metabolize this drug, contributes to expanding the mechanistic understanding of drug-
282 microbiome interactions. Moreover, we extended previous observations on the bacterial
283 inactivation of tacrolimus *(13)* by identifying related drug metabolites of sirolimus and
284 everolimus, indicating a similar microbial inactivation process.

285 The challenges we faced in predicting microbial drug metabolism *in vitro* and *ex vivo*
286 illustrate that predicting gut microbial metabolism of immunosuppressants in the clinical setting
287 may be similarly complex. Additionally, our results suggest that the difficulty of predicting gut
288 microbial drug metabolism may vary substantially among different immunosuppressants. While
289 some compounds may only require taxonomic information, for others mechanistic information
290 on metabolizing enzymes may be necessary. Moreover, the experimental identification of one
291 metabolizing enzyme, even in an abundant gut commensal, may not be sufficient for a

292 community-level understanding of drug metabolism, as suggested by inconsistencies between
293 experimentally and model-identified key species. Such inconsistencies may however also arise
294 from technical limitations inherent in both approaches (such as small sample size, Fig. 6C).
295 Specifically, our work revealed limitations of using sequence similarity alone to predict
296 community or species activity. While structural enzyme features may be used to refine homology
297 searches aimed at quantifying the genomic abundance of similar drug-metabolizing genes in the
298 community, the small size of our data set precludes a conclusive evaluation and rather highlights
299 the challenges of predicting community metabolism. This is especially true for prevalent enzyme
300 families, such as hydrolases, which are difficult to computationally quantify comprehensively in
301 the microbiome as demonstrated with MMF.

302 In summary, our work adds to the increasing evidence for the influence of the gut microbiome on
303 the metabolism of immunosuppressive drugs, but also highlights the difficulties in clinical
304 translation of this knowledge. Nevertheless, by integrating our *in vitro* and *ex vivo* data with data
305 from clinical studies, we may facilitate approaches towards personalized immunosuppression,
306 recognizing the significant, but previously underappreciated role of the gut microbiome in
307 individual variations in drug metabolism.

308 MATERIALS AND METHODS

309 Chemicals

310 Tested drugs were purchased from Sigma Aldrich, Santa Cruz Biotechnology or TCI as listed in
311 Table S20. LC–MS-grade solvents were purchased from Guyer and other chemicals from Sigma
312 Aldrich.

313 Human fecal material

314 The study was approved by the Ethics Committee of the Medical Faculty of Heidelberg
315 University (Study-ID: S-374/2021) and EMBL's Bioethics Internal Advisory Board. It was
316 performed in accordance with the World Medical Association Declaration of Helsinki Ethical
317 Principles in the currently valid version. All samples were stored in the Zimmermann laboratory,
318 using identifier numbers that are not associated with study volunteer names or other identifying
319 information. Study volunteers were recruited at EMBL Heidelberg or the University Children's
320 Hospital Heidelberg. Table S1 gives an overview of all collected information of study
321 volunteers. After collection samples were stored at 4˚C and processed within < 18 hours under
322 anaerobic conditions. Processing included the 1:1 addition of 40% glycerol in PBS followed by
323 homogenization using the IKA ULTRA-TURRAX blender (VWR, Cat.Nr. 4312897). Samples
324 were then aliquoted into 1 ml cryovials and stored at -80˚C until further analysis.

325 **Microbial culture conditions**

326 *Anaerobic culture conditions.*

327 Anaerobic cultivation was carried out as previously described *(7)*, using an anaerobic chamber
328 (Coy Laboratory Products) with a gas mix of 20% CO2, 10% H2, and 70% N2. Solid cultures were
329 grown on Brain-heart infusion (BHI; Becton Dickinson) agar with 10% horse blood. Liquid
330 cultures of individual strains and fecal communities were grown in gut microbiota medium (GMM)
331 *(23)*.

332 *Aerobic culture conditions*.

333 For molecular cloning, *E. coli* strains were aerobically cultured at 37°C in LB medium and on LB
334 agar plates with kanamycin (50µg/ml), following previously established protocols *(7)*.

335 **Mass spectrometry analysis of drugs and metabolites**

336 *Extraction of liquid samples.*

337 Liquid samples were processed for LC–MS analysis by organic solvent extraction as previously
338 described *(7)*. In brief, a mixture of acetonitrile:methanol (1:1) was introduced at -20°C following
339 the addition of an internal standard mix, which included sulfamethoxazole, caffeine, ipriflavone,
340 warfarin, and lisinopril, each at a final concentration of 80 nM. For samples derived from transwell
341 assays, the internal standard mix excluded warfarin and lisinopril.

342 *LC–MS analysis.*

343 Analysis was performed utilizing reversed-phase chromatography on an InfinityLab Poroshell
344 HPH-C18 column (2.1x100 mm, 1.9 µm) with an Agilent 1200 Infinity UHPLC system. Mobile
345 phases A (water with 0.1% formic acid) and B (methanol with 0.1% formic acid) were used, and
346 the column was maintained at 45°C. A 5 µl sample was injected with an initial 100% phase A at a
347 flow rate of 0.4 ml/min, followed by a linear gradient to 95% phase B over 5.5 minutes at the same
348 flow rate. The qTOF (Agilent 6546) was operated in positive scanning mode (50–1,000 m/z), with
349 source settings of 3,500 V for VCap, 2,000 V for nozzle voltage, a gas temperature of 225°C, a
350 drying gas flow of 13 l/min, nebulizer pressure at 20 psig, and sheath gas settings of 225°C
351 temperature and 12 l/min flow.

352 **Analysis of drug metabolism screen**

353 *Identification of metabolized drugs.*

354 A combined approach using both Fold Change (FC) and Area Under the Curve (AUC) was used
355 to determine whether a drug was degraded. Fold change was used as reported previously *(7)*. In
356 brief, for each community, drug fold changes were calculated between each time point and 0 h in
357 the 4 pools that contained a specific drug, and between these drug-containing pools and the non-
358 drug controls. Statistical significance of the drug intensity differences was assessed with One-Way
359 Permutation Test based on 9999 Monte-Carlo resampling (oneway_test function in R from the

360 coin package) ***(24)***, and P values were FDR-corrected for multiple hypotheses testing using the
361 Benjamini-Hochberg procedure (p.adjust function in R with method parameter set to "fdr"). To
362 account for fast drug metabolism (within seconds after exposure), fold changes to control at time
363 point 0 were used for drug and community/strain combinations for which (i) log2(fold change to
364 control at t = 0) < −2; (ii) FDR-corrected P value (fold change to control at t = 0) < 0.05; and (iii)
365 log2(fold change to control at t = 0) < log2(fold change at t = 12 h to t = 0). To account for
366 variability in drug measurements, for each drug an adaptive fold-change threshold was calculated
367 as either (i) (25%) or (ii) (mean + 2 s.d. of the fold changes, for which log2(fold change at t = 12
368 h to t = 0 h) > 0, to account for measurement noise), whichever was greater. Area Under the Curve
369 was used as follows: AUC was computed using the R DescTools::AUC function on normalized
370 and scaled areas for each of the sample, drug and pool combination. To account for variability in
371 drug measurements, for each drug an adaptive AUC threshold was calculated as either (i) the
372 average AUC computed on the control samples for the same drug, diminished of the desired
373 percentage of metabolism (here, 25%), or (ii) the average AUC computed on the control samples
374 for the same drug, diminished of two times their standard deviation whichever was smaller. A
375 sample was reported as metabolized if its median AUC was less than the AUC threshold. Once
376 both FC and AUC were used to assess drug degradation, if they returned two different results for
377 the same drug-sample combination (*i.e.*, one identified it as degrading, the other as non-degrading),
378 the following approach was used: (i) if AUC was claiming the sample as non-degrading the drug,
379 then the FC result is kept only if either it is a quickly degrading drug or the fold change its double
380 the requested FC; (ii) if AUC is claiming the sample as degrading the drug, then the AUC result is
381 kept only if the corresponding FC is above 1 due to measurement noise at the 12h time point.
382 *Identification of drug metabolites.*

383 We identified drug metabolite formation using linear mixed effects models predicting metabolite
384 intensity using time and a random intercept for replicates. We assigned buildup if Benjamini-
385 Hochberg corrected P value was < 0.1. To ensure the accuracy of metabolite intensity
386 measurements, we adjusted for background noise by subtracting the baseline signal from the
387 measured area before fitting the models.

388 **Preparing gain-of-function libraries, strain pooling and hit validation**

389 Plasmids and primers are listed in Table S21 and S22.

390 *Preparing gain-of-function library.*

391 Heterologous expression libraries were prepared as previously described *(7)*. In brief, genomic
392 DNA was extracted from overnight cultures of the source bacterial strain *B. uniformis (25)*. DNA
393 was fragmented into 2–8 kb pieces using focused ultrasonication (Covaris E220 with miniTUBE
394 red). DNA Fragments were subsequently cloned into a PCR-linearized pZE21 expression vector
395 (primers 1 and 2) through blunt-ended ligation (Thermo Fisher Rapid DNA Ligation kit). Ligated
396 products were run on a 0.5% agarose gel to isolate fragments between 5 and 10 kb, which were
397 then purified with a gel extraction kit (Qiagen). Ligation products were transformed into *E. cloni*
398 10G Elite competent cells (Lucigen) via electroporation. Colonies that grew overnight were
399 selected and arrayed in a 384-well plate containing LB medium with kanamycin, assisted by a
400 colony-picking robot (Singer Rotor). Inoculated plates were incubated overnight at 37°C, then
401 duplicated onto LB agar plates with kanamycin and stored at -70°C for preservation.

402 *Gain-of-function screen.*

403 Screening of the gain-of-function libraries was carried out as previously described *(7)*. In brief, we
404 first pooled all 384 colonies from a single library plate and resuspended them in diluted GMM
405 containing MMF (5μM). The suspension was incubated anaerobically at 37°C and samples were

406 collected at intervals of 0, 1, 2, 4, 6, 8, 12, and 24 hours during incubation. Pools showing the
407 ability to metabolize MMF were then transferred to a new 384-well plate and cultured aerobically
408 for 12 hours at 37°C. We identified three active plates and we created pools of each row and
409 column for further investigation. Active clones that metabolized MMF were isolated, and four
410 individual colonies from each were re-evaluated for their MMF-metabolizing capability. Once
411 confirmed, these clones underwent Sanger sequencing to identify the genetic inserts using primers
412 3 and 4.

413 *Hit validation by targeted gene expression in E. coli.*

414 To confirm the activity of the identified genes, their sequences were amplified using PCR with
415 primers 5 and 6, cloned into the pZE21 expression vector via Gibson cloning (NEBuilder HiFi
416 DNA Assembly Kit from NEB), and then transformed into *E. cloni* 10G Elite cells by
417 electroporation. The resulting bacterial strains were further tested for MMF metabolization.

418 **Construction of *B. uniformis* targeted mutant and complementation strains.**

419 Bacterial strains, plasmids, and primers are listed in Tables S6, 21 and S22. Gene deletions and
420 complementations were carried out as previously described *(26)*. The BACUNI_RS05305 gene
421 was deleted from *B. uniformis* (DSM6597) using a pLGB13 suicide plasmid. The plasmid was
422 constructed using primer numbers 7-14. For introducing the plasmid into *B. uniformis*,
423 conjugation with *E. coli* S17-pir was utilized. *E. coli* S17-pir containing plasmid
424 pLGB13_MMF_KO_BACUNIRS05305 was cultured aerobically in liquid LB medium
425 supplemented with ampicillin (100µg/ml), while *B. uniformis* was grown anaerobically in BHI
426 medium enriched with hematin (0.5 mg/mL) and menadione (0.1 mg/mL). Following growth,
427 both bacterial cultures were pelleted by centrifugation, resuspended, and mixed in 50 µL of BHI
428 medium supplemented with hematin and menadione. This mixture was then spotted onto a BHI-

429 blood agar plate and incubated aerobically at 37°C for 12-24 hours. After incubation, the
430 bacterial culture was transferred onto BHI agar plates containing erythromycin (5 µg/mL) and
431 gentamicin (200 µg/mL) to select for transconjugant *B. uniformis* clones. After 2 days of
432 anaerobic incubation, colonies were picked and further screened for second recombination events
433 on BHI plates containing anhydrotetracycline (100 ng/mL) for counterselection. Verification of
434 scare-less gene knock outs was performed using PCR with primers 14 and 15. Gene
435 complementation at different expression levels using engineered phage promotors were
436 performed with primer numbers 16-19 as described before *(7, 27)*.

437 **Epithelial transport assay.**

438 Caco-2 cells were obtained from Sigma (Cat no. 86010202) at passage 9. Cells used in this study
439 were not passaged more than 20 times. Transwell inserts were obtained from Millicell, and were
440 used in combination with 24-well plates (Thermo Fisher). The Caco-2 cells were grown in T75
441 flasks at 37˚C in an incubator with an atmosphere of 5% CO2. The cells were grown using
442 Dulbecco's modified Eagle medium (DMEM) (Gibco, 41965-039) with 4.5 g/liter D-glucose, 584
443 mg/liter L-glutamine, 1% penicillin/streptomycin, 1% amphotericin B, and 10% fetal bovine
444 serum. The medium in the flasks was changed every 3 days. At 90% confluence, the cells were
445 passaged using incubation with 0.5% trypsin for 5 minutes at 37˚C after washing the cells with
446 PBS. Cells were then seeded into the transwell inserts (pore size 0.4 µm) at 10,000 cells/well
447 (Merck). The transwells with the Caco-2 cells were used only after >21 days post-seeding to allow
448 for the establishment of a stable monolayer. During this post-seeding period, the media was
449 changed every 3 days. For each assay, the TEER of each monolayer was measured, to ensure the
450 stability and permeability of each monolayer. Transwells were only used when the TEER
451 measurement was above 2,083 Ohm/cm2 per well. The transwell inserts with the Caco-2

452 monolayer were washed 2 times with Hank's Buffered Salt Solution (HBSS), before adding the
453 sterile supernatant from the bacterial strains, or the single compounds in solution to the apical or
454 basolateral side. Small volumes of both the apical and basolateral side (10 uL) were taken every
455 30 minutes and immediately stored at -70°C until metabolite extraction. Time points were taken
456 for 5 hours, whereafter the cells were washed 3 times with HBSS and media was added to the cells,
457 on the apical side containing a viability dye (Promega, G8080). After an overnight incubation, the
458 apical media was transferred to a separate 96-well plate and fluorescent signal was measured.
459 Quantification of the compound concentrations in the epithelial transport assays was based on a
460 dilution series of chemical standards spanning 0.001 to 10 µM. The effective permeability
461 coefficients from the receiver compartments were calculated as described previously *(18)*. In short,
462 the following formula was used: $P_{eff} = \frac{V_R}{AC_0} dC/dt$. Here, V_R is the volume of the receiver
463 compartment, A the transwell surface area, C_0 the initial concentration of the solute in the receiver
464 compartment, and dC/dt the slope of the first 240 minutes of the concentration of the solute in the
465 receiver compartment. Statistical analysis and plotting were performed in RStudio Version 4.4.2.

466 **Metagenomic sequencing analysis**

467 *Sample preparation and sequencing.*

468 Fecal DNA was extracted from a biomass pellet of 1.5 ml of microbial community cultures using
469 the ZymoBIOMICS DNA Miniprep Kit (D4300). Library preparation and sequencing were
470 performed at the EMBL Genomics Core Facility at EMBL Heidelberg. The NEBNext Ultra II
471 DNA kit was used for the preparation of the metagenomic sequencing libraries. Sequencing was
472 performed on an Illumina NextSeq2000 instrument with a P3 flow-cell to target depth of 40 million
473 reads per sample.

474 *Taxonomic profiling*

475 Raw shotgun metagenomic reads were subjected to the following read cleaning protocol with
476 bbduk (bbmap-version 38.93): 1) low quality trimming on either side (qtrim = rl, trimq = 3), 2)
477 discarding of low-quality reads (maq = 25), 3) adapter removal (ktrim = r, k = 23, mink = 11, hadis
478 = 1, tpe = true, tbo = true; against the bbduk default adapter library) and 4) length filtering (ml =
479 45). The cleaned reads were screened for host contamination using kraken2 (version 2.1.2) against
480 the human hg38 reference genome with ribosomal sequences masked (SILVA 138). Microbial
481 abundance profiles were then generated using mOTUs3 with default settings *(28)*.

482 *Functional profiling*

483 Prior to functional profiling, raw shotgun metagenomics reads were subjected to the same read
484 cleaning protocol as described in the section 'Taxonomic profiling'. Preprocessed reads were
485 then mapped to the human gut specific Global Microbial Gene Catalogue (GMGC) *(29)* using
486 BWA-MEM (0.7.17) with default parameters. Here, a reduced GMGC catalog excluding very
487 rare genes was used (described in *(30)*). Alignments were filtered to >45bp alignment length and
488 >97% sequence identity and profiled with gffquant version v2.9.1
489 (https://github.com/cschu/gff_quantifier). Reads aligning ambiguously to multiple genes
490 contributed proportionally.

491 **Predicting community microbial activity from gene- and taxon abundances**

492 In order to predict community-wide metabolic activity, we built Random Forest models to infer
493 observed drug degradation (measured via AUC, defined above) using either community mOTU-
494 level taxonomic profiles or gene-level functional profiles. For model building, we used 38
495 metagenomic samples (19 anaerobic and 19 microaerobic). Models were trained and evaluated in
496 a leave-two-samples-out manner where samples from the same donor were always kept together
497 in the training or test set. We evaluated four different feature sets defined as follows: 'Active

498 species' correspond to those mOTUs that contain a metabolically active strain. Mapping between
499 strains and mOTUs was achieved by extracting mOTUs marker genes from strain genomes and
500 subsequent assignment to mOTUs (using functionality provided with mOTUs3
501 https://github.com/motu-tool/mOTUs-extender). 'Abundant species' features were derived from
502 relative abundances of the 345 mOTUs with prevalence > 20% and maximum abundance across
503 samples of > 0.1%. 'Characterized genes' correspond to the GMGC clusters that are similar to an
504 enzyme with established metabolic activity (Table S18), where similarity was defined as gene
505 sequences in the GMGC being at least 40% similar over at least 70% of their length, determined
506 using DIAMOND *(31)*. 'All genes' corresponds to all ~9M GMGC genes found in the *ex vivo*
507 communities. To reduce this feature set to a manageable size before Random Forest training, we
508 calculated feature-wise correlations to the label on each training set and retained only the best-
509 correlated 1000 features as input to the Random Forest. For all predictions, input features were
510 standardized (to mean 0 and standard deviation 1) before training the model.
511 In order to define the set of most important features for all evaluated models (shown in Fig. 6
512 and S6), we trained models by recursive feature addition, *i.e.*, successively adding the most
513 predictive features (computed via out-of-bag-estimated % increase in MSE upon feature
514 permutation using the RandomForest function in R) until the model based on this small set of top
515 features achieved a test performance larger than 90% of the full model. This was conducted for
516 each leave-two-samples-out fold individually, which resulted in a fold-specific set of top
517 features, across which information was aggregated to display feature importance (shown in Fig.
518 6 and S6).
519 **Predicting drug-metabolizing capacity of bacterial strains**

520 In order to facilitate prediction of MMF-metabolic activity of gut communities, homologs of
521 BACUNI_RS05305 were identified in the genomes of 43 bacterial strains using a BLAST *(32)*
522 search using 50% sequence identity and 50% query coverage as cutoffs. We excluded *B.*
523 *uniformis* from this search as the query enzyme originated from this organism. In total, 32
524 putative homologs were detected in 18 strains. To structurally investigate the active sites of these
525 homologs, Alphafold2 v2.3.2 *(33, 34)* was used with default parameters to predict five models
526 for each of the putative homologs. The highest confidence model was relaxed and then used for
527 further analysis. Conservation of the catalytic triad and the oxyanion hole residues was assessed
528 through a multiple sequence alignment of all 32 homologs using MUSCLE v5 *(35)*. After
529 alignment on catalytic residues, accessibility and polarity of the binding site was assessed by
530 visual inspection. We then used structural features around the catalytic site to obtain structure-
531 informed activity predictions. A fully accessible substrate binding site was considered necessary
532 to predict an enzyme to be active. Additionally, either a fully apolar binding site (no charged,
533 surface-exposed residues within 5A) or a binding site featuring both charged residues and large
534 apolar residues composing the oxyanion hole at position 191 was deemed necessary for activity
535 against MMF. Finally, we predicted a strain to be active against MMF, if a single putative
536 homolog in this strain was predicted active. As a result, of the 32 detected homologs from 18
537 strains, 24 homologs from 11 strains were classified as active using this structurally refined
538 prediction. Images of structures were generated using open source PyMOL (PyMOL Molecular
539 Graphics System, Version 2.3.0, Schrödinger, LLC.)
540

541 **List of Supplementary Materials**

542 Fig. S1 to S8

543 Tables S1 to S22

544

545 **References and Notes**

546 1. A. Rana, A. Gruessner, V. G. Agopian, Z. Khalpey, I. B. Riaz, B. Kaplan, K. J. Halazun, R.
547 W. Busuttil, R. W. G. Gruessner, Survival Benefit of Solid-Organ Transplant in the United
548 States. *JAMA Surg* **150**, 252 (2015).

549 2. M. Coemans, C. Süsal, B. Döhler, D. Anglicheau, M. Giral, O. Bestard, C. Legendre, M.-P.
550 Emonds, D. Kuypers, G. Molenberghs, G. Verbeke, M. Naesens, Analyses of the short- and
551 long-term graft survival after kidney transplantation in Europe between 1986 and 2015. *Kidney*
552 *International* **94**, 964–973 (2018).

553 3. S. Bergan, M. Brunet, D. A. Hesselink, K. L. Johnson-Davis, P. K. Kunicki, F. Lemaitre, P.
554 Marquet, M. Molinaro, O. Noceti, S. Pattanaik, T. Pawinski, C. Seger, M. Shipkova, J. J. Swen,
555 T. van Gelder, R. Venkataramanan, E. Wieland, J.-B. Woillard, T. C. Zwart, M. J. Barten, K.
556 Budde, M.-T. Dieterlen, L. Elens, V. Haufroid, S. Masuda, O. Millan, T. Mizuno, D. J. A. R.
557 Moes, M. Oellerich, N. Picard, L. Salzmann, B. Tönshoff, R. H. N. van Schaik, N. T. Vethe, A.
558 A. Vinks, P. Wallemacq, A. Åsberg, L. J. Langman, Personalized Therapy for Mycophenolate:
559 Consensus Report by the International Association of Therapeutic Drug Monitoring and Clinical
560 Toxicology. *Therapeutic Drug Monitoring* **43**, 150–200 (2021).

561 4. M. Brunet, T. van Gelder, A. Åsberg, V. Haufroid, D. A. Hesselink, L. Langman, F. Lemaitre,
562 P. Marquet, C. Seger, M. Shipkova, A. Vinks, P. Wallemacq, E. Wieland, J. B. Woillard, M. J.
563 Barten, K. Budde, H. Colom, M.-T. Dieterlen, L. Elens, K. L. Johnson-Davis, I. MacPhee, S.
564 Masuda, B. S. Mathew, O. Millán, T. Mizuno, D.-J. A. R. Moes, C. Monchaud, O. Noceti, T.

565 Pawinski, N. Picard, R. van Schaik, C. Sommerer, N. T. Vethe, B. de Winter, U. Christians, S.
566 Bergan, Therapeutic Drug Monitoring of Tacrolimus-Personalized Therapy: Second Consensus
567 Report. *Ther Drug Monit* **41**, 47 (2019).

568 5. N. Shuker, T. van Gelder, D. A. Hesselink, Intra-patient variability in tacrolimus exposure:
569 Causes, consequences for clinical management. *Transplantation Reviews* **29**, 78–84 (2015).

570 6. L. M. Andrews, Y. Li, B. C. M. De Winter, Y.-Y. Shi, C. C. Baan, T. Van Gelder, D. A.
571 Hesselink, Pharmacokinetic considerations related to therapeutic drug monitoring of tacrolimus
572 in kidney transplant patients. *Expert Opinion on Drug Metabolism & Toxicology* **13**, 1225–1236
573 (2017).

574 7. M. Zimmermann, M. Zimmermann-Kogadeeva, R. Wegmann, A. L. Goodman, Mapping
575 human microbiome drug metabolism by gut bacteria and their genes. *Nature* **570**, 462–467
576 (2019).

577 8. B. Javdan, J. G. Lopez, P. Chankhamjon, Y.-C. J. Lee, R. Hull, Q. Wu, X. Wang, S.
578 Chatterjee, M. S. Donia, Personalized Mapping of Drug Metabolism by the Human Gut
579 Microbiome. *Cell* (2020), doi:10.1016/j.cell.2020.05.001.

580 9. A. A. Verdegaal, A. L. Goodman, Integrating the gut microbiome and pharmacology. *Sci.*
581 *Transl. Med.* **16**, eadg8357 (2024).

582 10. M. Zimmermann, K. R. Patil, A. Typas, L. Maier, Towards a mechanistic understanding of
583 reciprocal drug–microbiome interactions. *Molecular Systems Biology* **17**, e10116 (2021).

584 11. K. A. Lee, Cross-cohort gut microbiome associations with immune checkpoint inhibitor
585 response in advanced melanoma. *Nature Medicine* , 28.

586 12. M. R. Taylor, K. L. Flannigan, H. Rahim, A. Mohamud, I. A. Lewis, S. A. Hirota, S. C.
587 Greenway, Vancomycin relieves mycophenolate mofetil–induced gastrointestinal toxicity by
588 eliminating gut bacterial β-glucuronidase activity. *Science Advances* **5**, eaax2358 (2019).

589 13. Y. Guo, C. M. Crnkovic, K.-J. Won, X. Yang, J. R. Lee, J. Orjala, H. Lee, H. Jeong,
590 Commensal gut bacteria convert the immunosuppressant tacrolimus to less potent metabolites.
591 *Drug Metabolism and Disposition* , dmd.118.084772 (2018).

592 14. G. P. Donaldson, S. M. Lee, S. K. Mazmanian, Gut biogeography of the bacterial microbiota.
593 *Nature Reviews Microbiology* **14**, 20–32 (2016).

594 15. S. Devendran, S. M. Mythen, J. M. Ridlon, The *desA* and *desB* genes from *Clostridium*
595 *scindens* ATCC 35704 encode steroid-17,20-desmolase. *Journal of Lipid Research* **59**, 1005–
596 1014 (2018).

597 16. M. P. M. Letertre, N. Munjoma, K. Wolfer, A. Pechlivanis, J. A. K. McDonald, R. N.
598 Hardwick, N. J. Cherrington, M. Coen, J. K. Nicholson, L. Hoyles, J. R. Swann, I. D. Wilson, A
599 Two-Way Interaction between Methotrexate and the Gut Microbiota of Male Sprague–Dawley
600 Rats. *J. Proteome Res.* **19**, 3326–3339 (2020).

601 17. S. Lazarević, M. Đanic, H. Al-Salami, A. Mooranian, M. Mikov, Gut Microbiota Metabolism
602 of Azathioprine: A New Hallmark for Personalized Drug-Targeted Therapy of Chronic
603 Inflammatory Bowel Disease. *Front. Pharmacol.* **13**, 879170 (2022).

604 18. A. R. Hilgers, R. A. Conradi, P. S. Burton, Caco-2 Cell Monolayers as a Model for Drug
605 Transport Across the Intestinal Mucosa. *Pharmaceutical Research* **07**, 902–910 (1990).

606 19. L. Qian, H. Ouyang, L. Gordils-Valentin, J. Hong, A. Jayaraman, X. Zhu, Identification of
607 Gut Bacterial Enzymes for Keto-Reductive Metabolism of Xenobiotics. *ACS Chem. Biol.* **17**,
608 1665–1671 (2022).

609 20. A. L. Degraeve, V. Haufroid, A. Loriot, L. Gatto, V. Andries, L. Vereecke, L. Elens, L. B.
610 Bindels, Gut microbiome modulates tacrolimus pharmacokinetics through the transcriptional
611 regulation of ABCB1. *Microbiome* **11**, 138 (2023).

612 21. P. Li, R. Zhang, J. Zhou, P. Guo, Y. Liu, S. Shi, Vancomycin relieves tacrolimus-induced
613 hyperglycemia by eliminating gut bacterial beta-glucuronidase enzyme activity. *Gut Microbes*
614 **16**, 2310277 (2024).

615 22. Y. Guo, H. Lee, E. Edusei, S. Albakry, H. Jeong, J. R. Lee, Blood Profiles of Gut Bacterial
616 Tacrolimus Metabolite in Kidney Transplant Recipients. , 2.

617 23. A. L. Goodman, G. Kallstrom, J. J. Faith, A. Reyes, A. Moore, G. Dantas, J. I. Gordon,
618 Extensive personal human gut microbiota culture collections characterized and manipulated in
619 gnotobiotic mice. *Proc Natl Acad Sci U S A* **108**, 6252–6257 (2011).

620 24. T. Hothorn, K. Hornik, M. A. V. D. Wiel, A. Zeileis, Implementing a Class of Permutation
621 Tests: The **coin** Package. *J. Stat. Soft.* **28** (2008), doi:10.18637/jss.v028.i08.

622 25. A. L. Goodman, M. Wu, J. I. Gordon, Identifying microbial fitness determinants by insertion
623 sequencing using genome-wide transposon mutant libraries. *Nat Protoc* **6**, 1969–1980 (2011).

624 26. L. García-Bayona, L. E. Comstock, K. P. Lemon, Ed. Streamlined Genetic Manipulation of
625 Diverse *Bacteroides* and *Parabacteroides* Isolates from the Human Gut Microbiota. *mBio* **10**,
626 e01762-19 (2019).

627 27. W. R. Whitaker, E. S. Shepherd, J. L. Sonnenburg, Tunable Expression Tools Enable Single-
628 Cell Strain Distinction in the Gut Microbiome. *Cell* **169**, 538-546.e12 (2017).

629 28. H.-J. Ruscheweyh, A. Milanese, L. Paoli, N. Karcher, Q. Clayssen, M. I. Keller, J. Wirbel, P.
630 Bork, D. R. Mende, G. Zeller, S. Sunagawa, Cultivation-independent genomes greatly expand
631 taxonomic-profiling capabilities of mOTUs across various environments. *Microbiome* **10**, 212
632 (2022).

633 29. L. P. Coelho, R. Alves, Á. R. Del Río, P. N. Myers, C. P. Cantalapiedra, J. Giner-Lamia, T.
634 S. Schmidt, D. R. Mende, A. Orakov, I. Letunic, F. Hildebrand, T. Van Rossum, S. K. Forslund,
635 S. Khedkar, O. M. Maistrenko, S. Pan, L. Jia, P. Ferretti, S. Sunagawa, X.-M. Zhao, H. B.
636 Nielsen, J. Huerta-Cepas, P. Bork, Towards the biogeography of prokaryotic genes. *Nature* **601**,
637 252–256 (2022).

638 30. Q. R. Ducarmon, N. Karcher, H. L. P. Tytgat, O. Delannoy-Bruno, S. Pekel, F. Springer, C.
639 Schudoma, G. Zeller, *Large-scale computational analyses of gut microbial CAZyme repertoires*
640 *enabled by Cayman* (bioRxiv 2024.01.08.574624, 2024;
641 https://doi.org/10.1101/2024.01.08.574624).

642 31. B. Buchfink, C. Xie, D. H. Huson, Fast and sensitive protein alignment using DIAMOND.
643 *Nat Methods* **12**, 59–60 (2015).

644 32. C. Camacho, G. Coulouris, V. Avagyan, N. Ma, J. Papadopoulos, K. Bealer, T. L. Madden,
645 BLAST+: architecture and applications. *BMC Bioinformatics* **10**, 421 (2009).

646 33. M. Varadi, S. Anyango, M. Deshpande, S. Nair, C. Natassia, G. Yordanova, D. Yuan, O.
647 Stroe, G. Wood, A. Laydon, A. Žídek, T. Green, K. Tunyasuvunakool, S. Petersen, J. Jumper, E.
648 Clancy, R. Green, A. Vora, M. Lutfi, M. Figurnov, A. Cowie, N. Hobbs, P. Kohli, G. Kleywegt,
649 E. Birney, D. Hassabis, S. Velankar, AlphaFold Protein Structure Database: massively
650 expanding the structural coverage of protein-sequence space with high-accuracy models. *Nucleic*
651 *Acids Research* **50**, D439–D444 (2022).

652 34. J. Jumper, R. Evans, A. Pritzel, T. Green, M. Figurnov, O. Ronneberger, K.
653 Tunyasuvunakool, R. Bates, A. Žídek, A. Potapenko, A. Bridgland, C. Meyer, S. A. A. Kohl, A.
654 J. Ballard, A. Cowie, B. Romera-Paredes, S. Nikolov, R. Jain, J. Adler, T. Back, S. Petersen, D.
655 Reiman, E. Clancy, M. Zielinski, M. Steinegger, M. Pacholska, T. Berghammer, S. Bodenstein,
656 D. Silver, O. Vinyals, A. W. Senior, K. Kavukcuoglu, P. Kohli, D. Hassabis, Highly accurate
657 protein structure prediction with AlphaFold. *Nature* **596**, 583–589 (2021).

658 35. R. C. Edgar, Muscle5: High-accuracy alignment ensembles enable unbiased assessments of
659 sequence homology and phylogeny. *Nat Commun* **13**, 6968 (2022).

660

661 **Acknowledgments:** We thank the Zeller and the Zimmerman labs for stimulating discussions of
662 our work and the EMBL GeneCore Facility for services and experimental advice.

663 **Funding:** Clinician Scientist Program by the Medical Faculty of Heidelberg (MBA)

664 Else Kröner Fresenius Foundation grant 2020_EKEA.62 (MBA)

State funds approved by the State Parliament of Baden-Württemberg for the Innovation Campus Health + Life Science Alliance Heidelberg Mannheim (NK)

Federal Ministry of Education and Research BMBF grant 031L0181A (GZ)

German Research Foundation grant 395357507 – SFB 1371 (GZ)

ERC grant GutTransForm ID 101078353 (MZ)

Author contributions: Conceptualization: MBA, DC, BT, GZ, MZ

Methodology: GZ, MZ

Investigation: MBA, NK, EM, RH, MG, AB

Visualization: MBA, NK, AB, EM, RH

Funding acquisition: MBA, BT, GZ, MZ

Project administration: MBA

Supervision: BT, GZ, MZ

Writing – original draft: MBA

Writing – review & editing: MBA, NK, AB, EM, RH, MG, DC, BT, GZ, MZ

Competing interests: Authors declare that they have no competing interests.

Data and materials availability: All data are available in the main text or the supplementary materials. Raw metagenomic sequencing data will be made available under the ENA project ID PRJEB74094. Taxonomic and functional profiles are available under the Zenodo accession ID 10895043. Raw metabolomics data will be made available in the MetaboLights repository, with accession number MTBLS9827. Code for analyzing data and generating figures are available on GitHub (https://github.com/zellerlab/gut-microbial-metabolism-of-immunosuppressants).

687 **Figures**

688 **Fig. 1.**

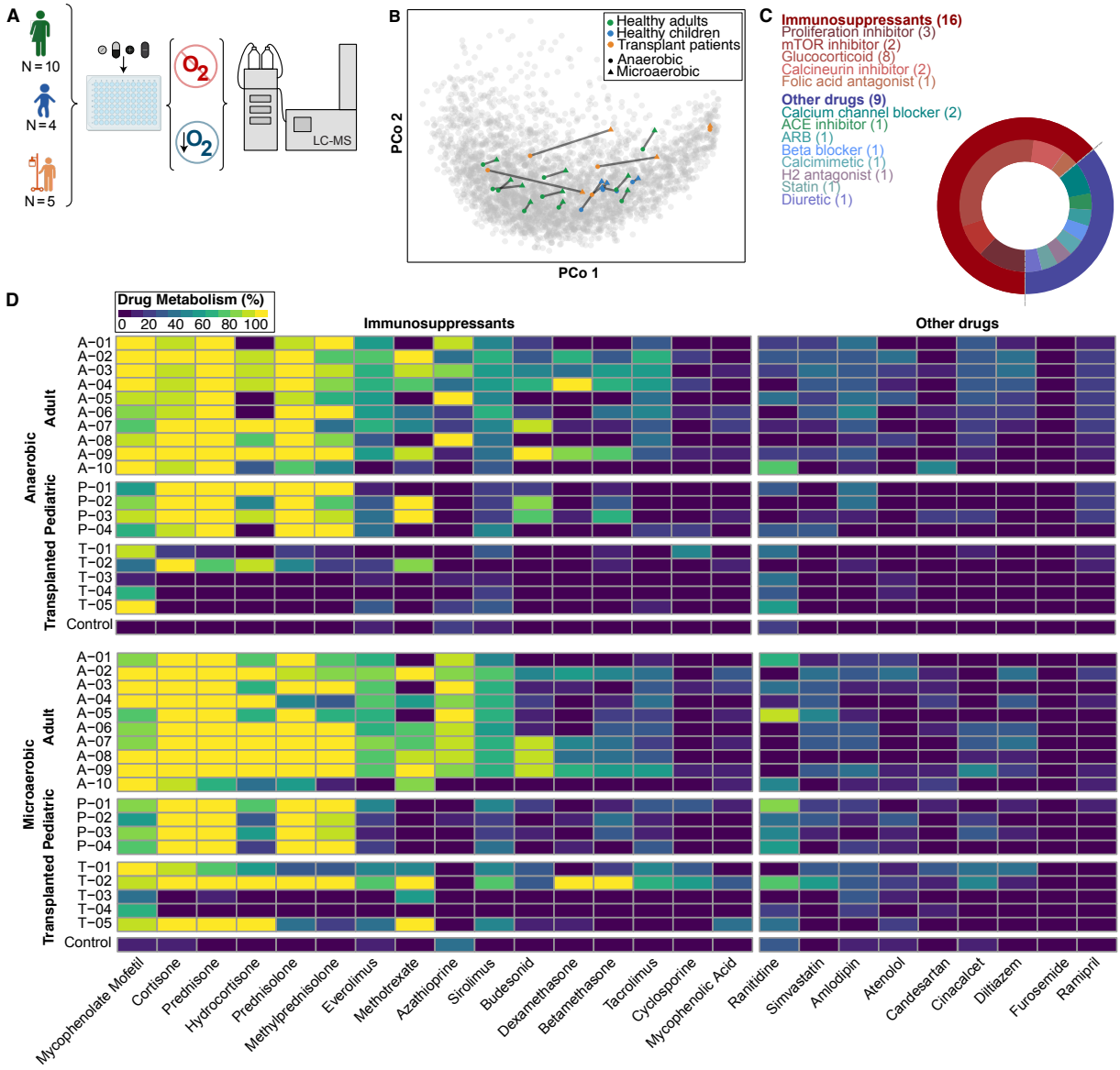

689

690 **Fig. 1. Drug metabolizing activity of human-derived gut microbial communities. (A)**

691 Schematic of the assay. **(B)** Principal Coordinates Analysis (PCoA) comparing the

692 composition of 38 human-derived gut microbial communities, cultivated under anaerobic

693 conditions for 8 hours before sequencing, to 3189 reference human gut microbial

694 metagenomes from 10 datasets in industrialized countries (corresponding to the
695 Westernized control samples used in *(30)*, Table S2). Circles and triangles denote the
696 tested communities, color-coded by population source (see inset). Gray circles represent
697 samples from reference metagenomes. Colored circles indicate samples cultivated
698 anaerobically, triangles represent microaerobically cultivated samples. Gray lines connect
699 *ex vivo* cultures originating from the same stool sample. **(C)** Overview of tested drug
700 classes, with the number of representatives tested indicated in brackets. Shades of red
701 represent immunosuppressants, while shades of blue denote other, non-
702 immunosuppressive drugs. Pie chart visualizes the proportion of each drug class among
703 all drugs tested. **(D)** Heat map depicting the metabolism of the 25 tested drugs by 38
704 human-derived gut microbial communities. The communities are arranged according to
705 the population source (adults, children, transplant patients). Drugs are ordered based on
706 drug class (immunosuppressant vs. other drugs) and observed metabolic activity.

Fig. 2.

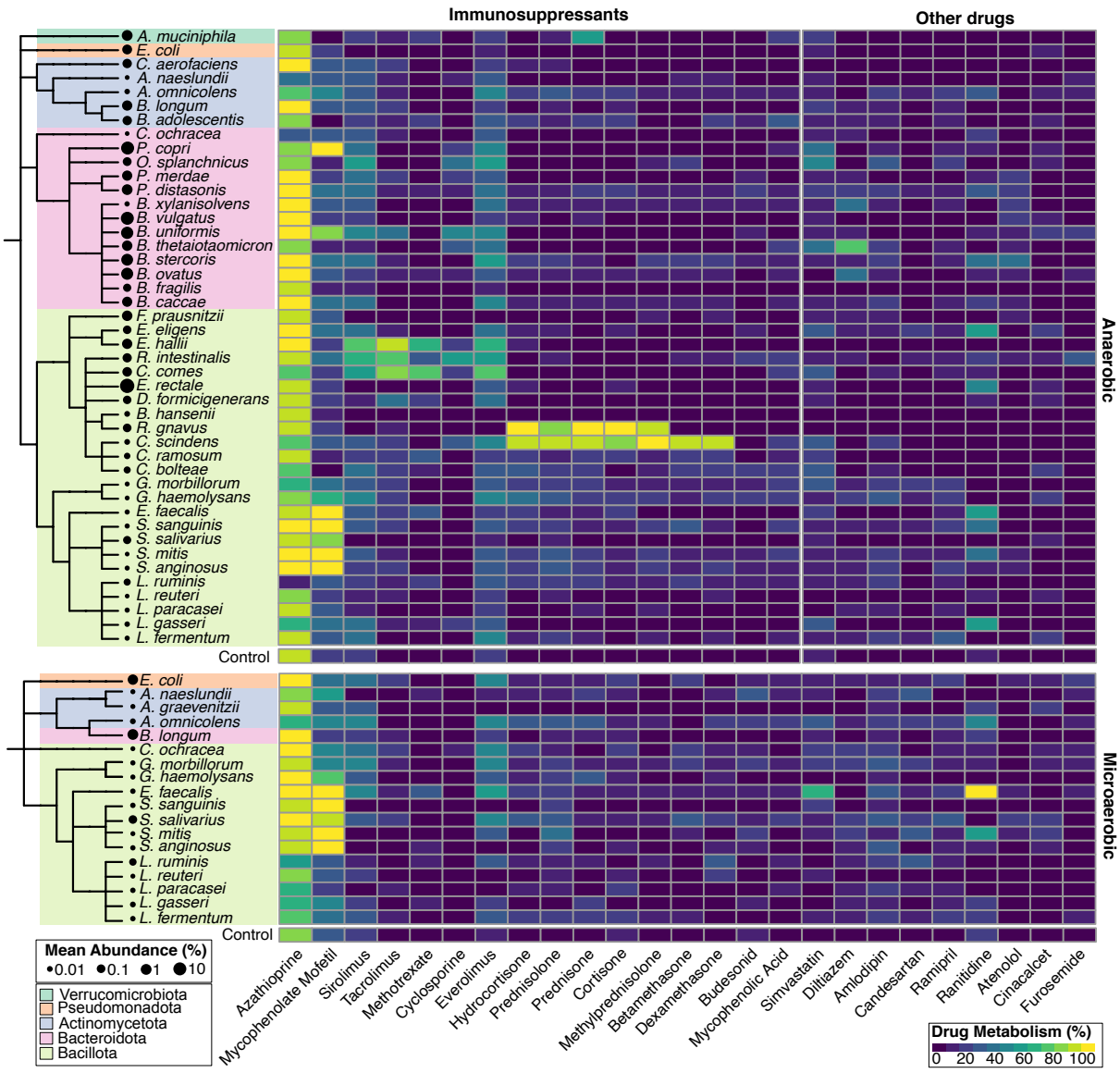

Fig. 2. Drug metabolizing activity of individual gut bacterial species. Heat map illustrating the metabolism of the 25 tested drugs by 45 individual gut bacterial species. The species are arranged taxonomically, with dendrogram color coding representing the respective phylum. Black dots indicate the mean abundance of each species estimated on the reference metagenomes (see Fig. 1B). Drugs are ordered based on drug class (immunosuppressant vs. other drugs) and observed metabolism.

716 **Fig. 3.**

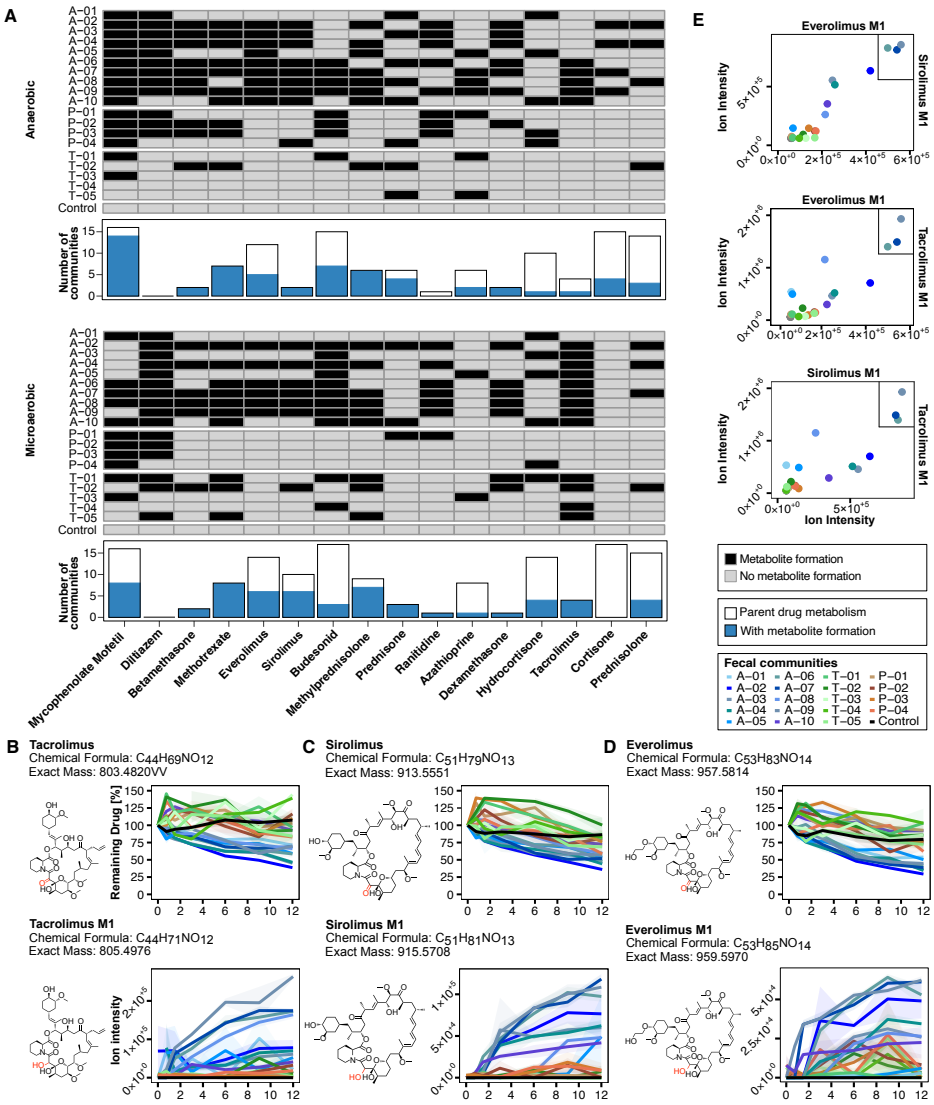

717

718 **Fig. 3. Identified drug metabolites in human-derived gut microbial communities. (A)** Heat

719 map illustrating microbial drug metabolite formation based on the parent drug (columns).

720 Bar outlines below the heat map depict the number of communities metabolizing a given

721 parent drug. Blue filled bars represent the number of communities where additional

722 metabolite formation was observed. Drugs are sorted based on metabolite formation,

723 while microbial communities are sorted based on the source population. **(B-D)** Chemical

724 structure and exact mass of parent drugs and their respective metabolites for tacrolimus,
725 sirolimus, and everolimus. Line plots depict the degradation of the parent drug and
726 formation of metabolites over time under anaerobic conditions, with individual
727 communities color-coded. Lines and shaded areas indicate the mean and s.e. of n=4 assay
728 replicates, respectively. **(E)** Scatterplots depict pairwise correlation of metabolite
729 formation of tacrolimus, everolimus, and sirolimus by human gut microbial communities
730 under anaerobic conditions, with color-coded circles representing individual
731 communities. In the upper right panel of each plot a black box highlights the same top
732 three communities most actively forming the metabolite.

733 **Fig. 4.**

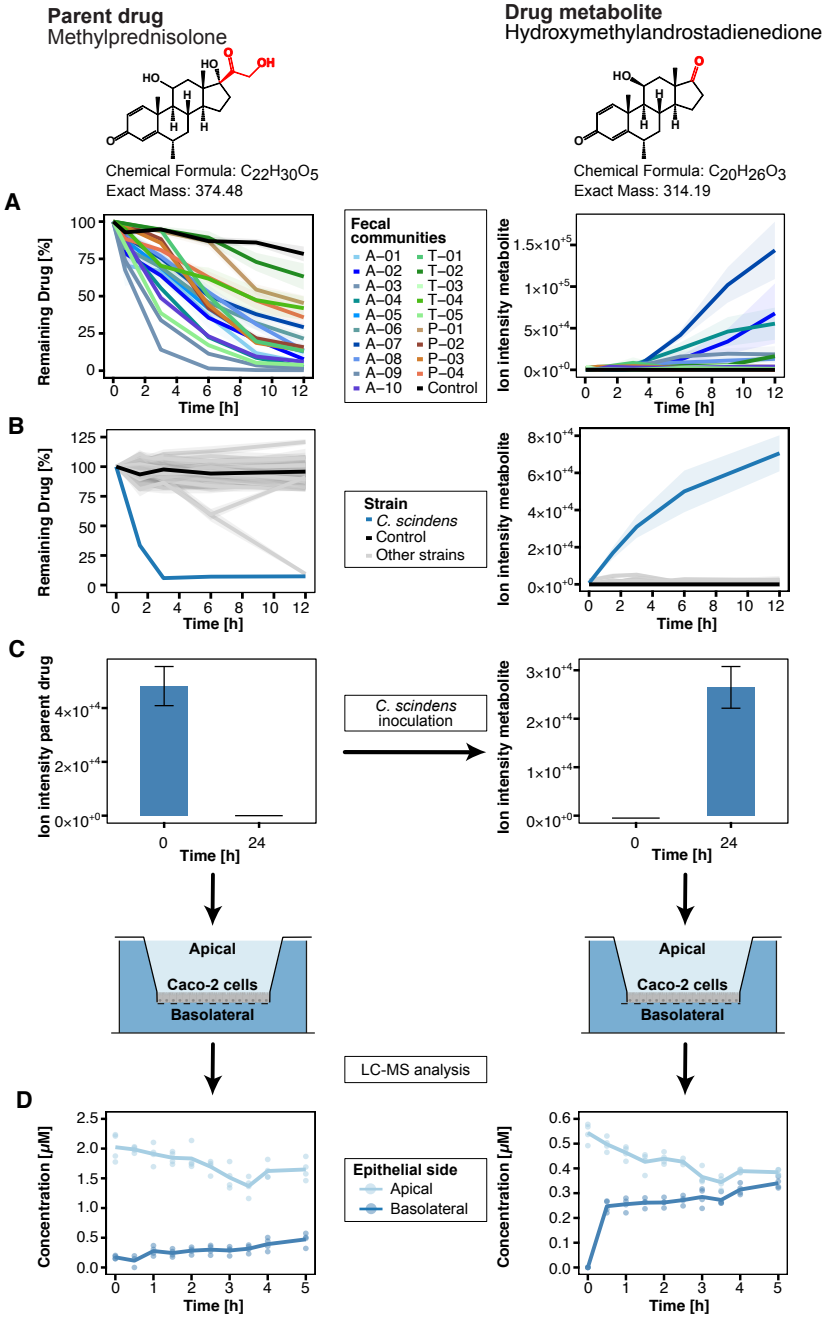

734

735 **Fig. 4. Epithelial transport characteristics of methylprednisolone and its microbial**

736 **metabolite. (A)** Gut microbial community metabolism of methylprednisolone (left) and

737 formation of its microbial metabolite hydroxymethylandrostadienedione (right) under

anaerobic conditions over time. Individual gut microbial communities are represented by color-coded lines. Lines and shaded areas depict the mean and s.e. of n=4 assay replicates, respectively. **(B)** Metabolism of methylprednisolone and formation of hydroxymethylandrostadienedione over time by individual bacterial species under anaerobic conditions. *C. scindens* used for metabolite accumulation shown in (C) is depicted by a blue line, while the other 44 species are shown with gray lines. Lines and shaded areas depict the mean and s.e. of n=4 assay replicates, respectively. **(C)** Barplot showing the ion intensity of methylprednisolone at the start of the *C. scindens* inoculation vs. after 24 hours, with metabolite buildup on the right. Barplots and error bars represent the mean and standard error of n=6 assay replicates. The lower panel includes a schematic of the transport assay, with light blue depicting the apical side of the epithelial Caco-2 monolayer and dark blue the basolateral side. **(D)** Line plot showing the concentration over time of methylprednisolone and its microbial metabolite hydroxymethylandrostadienedione on the apical (light blue) and basolateral side (dark blue), respectively. Lines represent the mean of n=4 assay replicates while circles represent individual measurements.

755 **Fig. 5.**

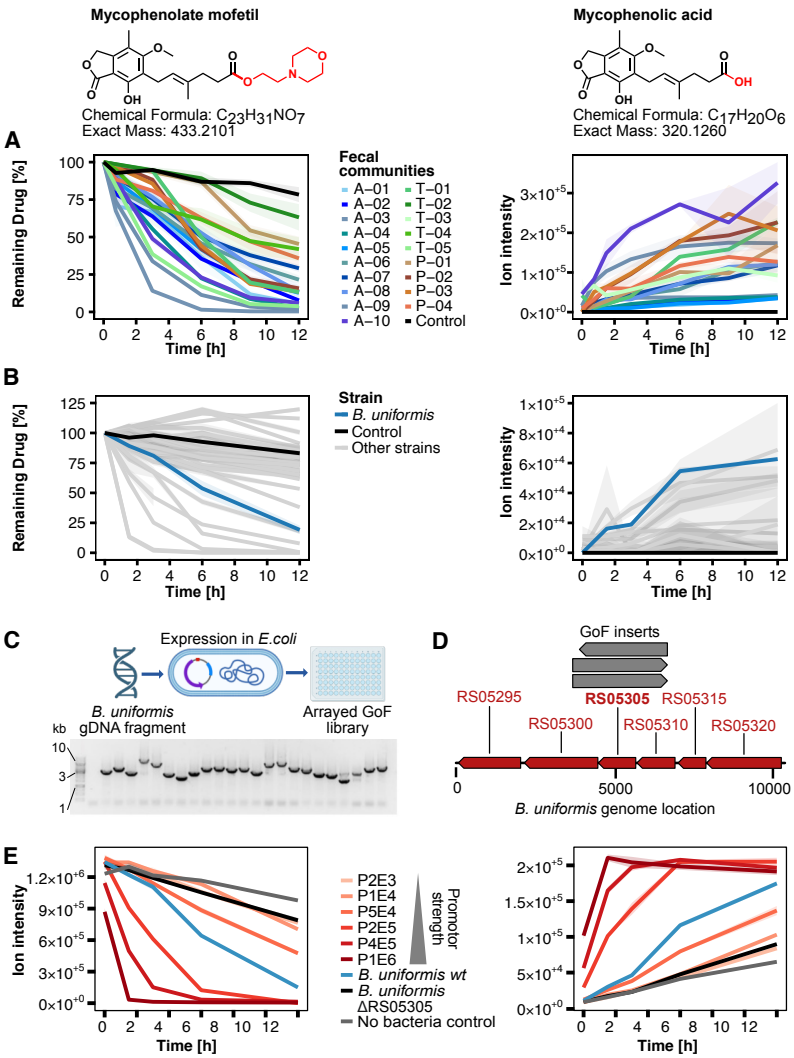

756

757 **Fig. 5. Identification of MMF-metabolizing bacterial enzyme. (A)** Gut microbial community

758 metabolism of mycophenolate mofetil (MMF, left) and formation of its microbial

759 metabolite mycophenolic acid (MPA, right) under anaerobic conditions over time.

760 Individual gut microbial communities are represented by color-coded lines. Lines and

761 shaded areas depict the mean and s.e. of n=4 assay replicates, respectively. **(B)**

762 Metabolism of MMF and formation of MPA over time by individual bacterial species

763 under anaerobic conditions. *B.uniformis* used for MMF-metabolizing enzyme

764 identification is depicted by a blue line, while the other 44 species are shown in
765 gray. Lines and shaded areas depict the mean and s.e. of n=4 assay replicates,
766 respectively. **(C)** Scheme for generation of an assayed gain-of-function (GoF) library and
767 insert size distribution of the *B. uniformis* library based on 23 randomly picked clones.
768 **(D)** Mapping of active insert sequences to the *B. uniformis* genome. **(E)** MMF-
769 metabolizing activity of *B. uniformis* wild-type, BACUNI_RS05305 knockout and
770 BACUNI_RS05305-complemented strains at different expression levels. Promoter
771 strengths are P1E6 > P4E5 > P2E5 > P5E4 > P1E4 > P2E3 *(27)*. Lines and shaded areas
772 depict the mean and s.e. of n=4 assay replicates, respectively.
773

774 **Fig. 6.**

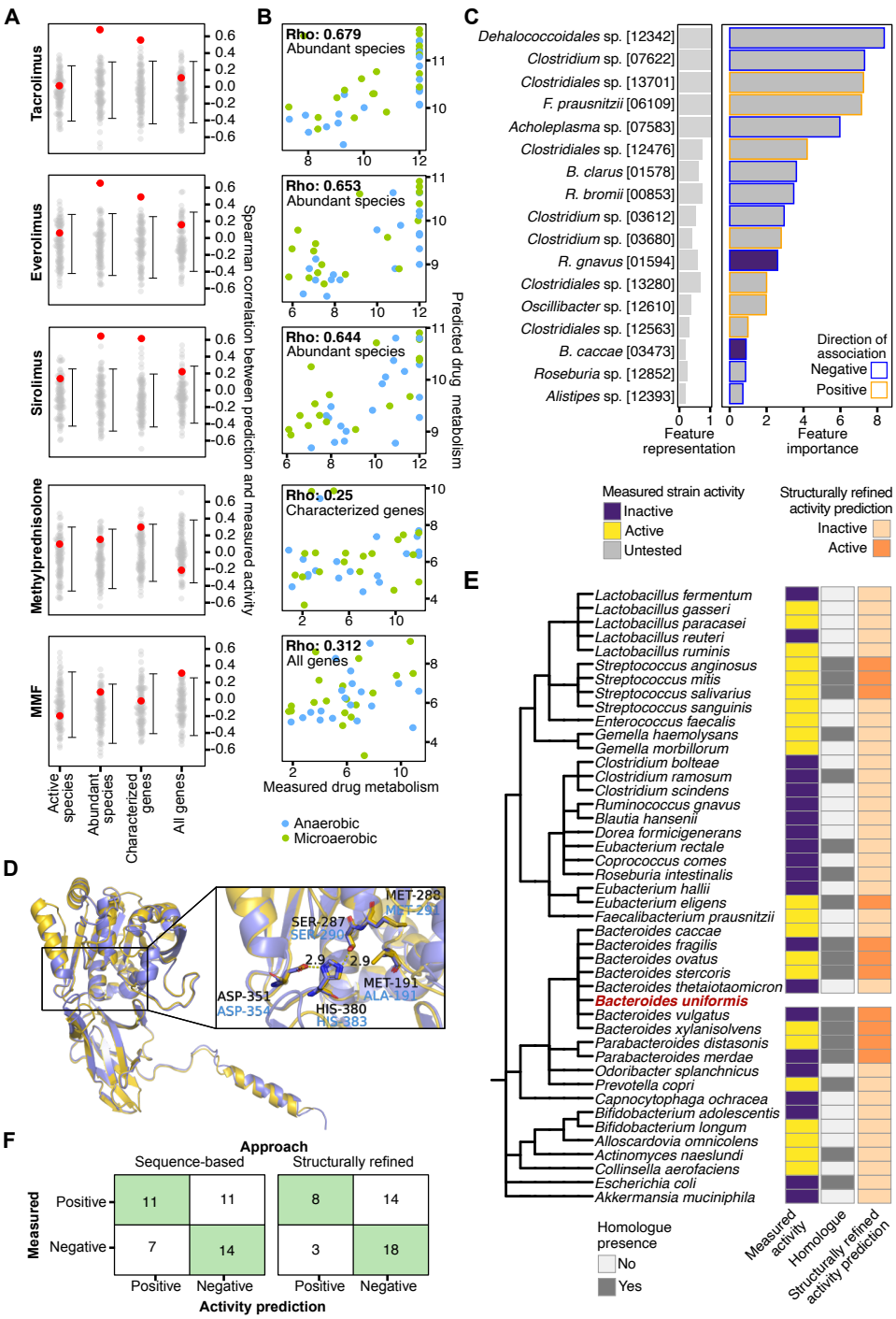

775

776 **Fig. 6. Predicting metabolic activity of microbial communities. (A)** Random Forest cross-

777 validation performances for four different models predicting community metabolism

778 based on different sets of taxon- and gene-abundance features (see text) are denoted by
779 red dots. These regression models predicted metabolic activity as quantified by the area
780 under the drug concentration curve over time (AUC capped at 12) and were evaluated in
781 terms of correlation between predicted and measured activity (see (B))**.** Gray dots
782 indicate performance estimates of 100 null models trained with permuted labels; 90%
783 confidence intervals are depicted by vertical lines with 5th and 95th percentile marked by
784 horizontal ticks. **(B)** Scatter plots of measured versus predicted drug metabolism shown
785 for the best-performing feature set evaluated in (A) for each drug (Spearman correlation
786 denoted by rho). **(C)** Feature Importance (quantified by increase in mean squared error
787 upon feature permutation, calculated on out-of-bag samples) of the most predictive taxa
788 in the 'abundant species' model for tacrolimus. Feature representation corresponds to the
789 fraction of cross-validated models that contain a given feature in their top feature set.
790 Only features contained in at least 20% of models are shown. Directionality of
791 association was inferred from the sign of the Spearman correlation between feature and
792 response variable (metabolic activity). Positive associations (orange outline) indicate that
793 a species is more abundant in communities with high metabolic activity. **(D)**
794 Superposition of Alphafold2 predicted models for BACUNI_RS05305 (yellow, active
795 enzyme) and BACUNI_RS05310 (blue, inactive enzyme) showing high structural
796 similarity. Both paralogs are composed of a catalytic α/β-hydrolase domain and an
797 immunoglobulin-like domain with an N-terminal signal peptide indicating secretion. The
798 enlarged view shows the binding site with residues of the catalytic triad (Ser-His-Asp)
799 and the oxyanion hole with hydrogen bonding distances of the catalytic triad given in
800 Angstrom. Met191 in the active paralog is mutated to alanine in the inactive one, likely

801 affecting (mycophenolate mofetil) MMF binding. **(E)** Taxonomy of the 44 species, for
802 which MMF metabolism was measured anaerobically (first column), alongside detection
803 of homologs to BACUNI_RS05305 (from *B. uniformis*, highlighted in red) inferred via
804 sequence similarity search (second column), or via manual scoring of structural features
805 of the active sites (see text) in these homologues (third column). **(F)** Contingency tables
806 for bacterial MMF metabolism of 43 species (excluding *B. uniformis*) comparing activity
807 prediction derived purely from sequence similarity-based homologue detection or
808 additional structural refinement against measured activity.